ACS APPLIED MATERIALS & INTERFACES

Research Article

www.acsami.org

Platinum Dendritic-Flowers Prepared by Tellurium Nanowires Exhibit High Electrocatalytic Activity for Glycerol Oxidation

Yunpeng Zuo, Long Wu, Kai Cai, Tingting Li, Wenmin Yin, Dian Li, Na Li, Jiawei Liu, and Heyou Han*

State Key Laboratory of Agricultural Microbiology, College of Science Huazhong Agricultural University, Wuhan 430070, P.R. China

Supporting Information

ABSTRACT: Dentritic Pt-based nanomaterials with enriched edge and corner atoms have recently attracted considerable attention as electrocatalysts. Meanwhile, Pt(111) facets are generally considered more active for the glycerol oxidation reaction (GOR). Thus, it is significant to construct the rational design and synthesis of dentritic Pt whose surface is mostly enclosed by {111} facets. Reported herein is a unique Pt-branched structure enriched by a large amount of valency unsaturated atoms prepared by the aggravation of the galvanic replacement strategy. The synthesis is developed to generate highly crystallized Pt nanoflowers using Te nanowires as a template. Furthermore, the electrochemical results show that Pt nanoflower is an excellent catalyst with higher mass activity and better structure stability than commercial Pt/C (20% Pt) for glycerol electro-oxidation. Besides, the template-broken approach could provide a novel potential way to synthesize Pt-based or other noble metals/alloys for their advanced functional applications.

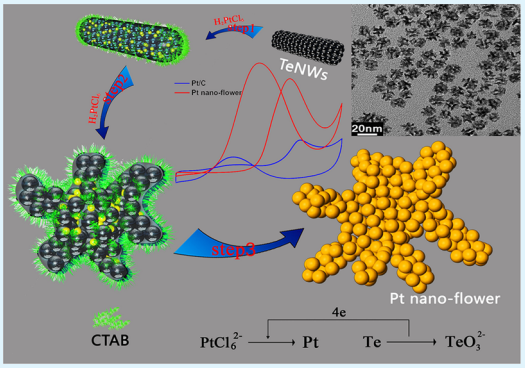

KEYWORDS: *platinum, dentritic-flowers, template-broken, glycerol, electro-oxidation*

INTRODUCTION

Noble metal nanomaterials have attracted extensive interest for electrocatalytic/catalytic applications because of their specific physicochemical properties.[1−4] As the most widely used commercial noble catalyst in fuel cells, the bulk of platinum (Pt) would have great effects on the prices of the products.[5,6] Meanwhile, the surface structure, which contains size, shape, and facets, has a strong impact on the properties of the Pt nanomaterials.[7−10] Since the highly branched structures with enriched edge and corner atoms provide more active surface areas and specific areas, dentritic nanomaterials have been widely studied as an effective approach to greatly enhance the catalytic activity of the Pt materials.[11,12] The previous work clearly showed the special structure acts as a key role of shape control in the efficient utilization of Pt nanomaterials.[7,13,14] As a type of important alcohol fuel, glycerol has a better security and higher theoretical energy density compared to methanol and ethanol.[15] What's more, glycerol could be obtained largely from the biomass system, which reveals the applied potential in the fuel cell industry.[15] Thus, it is significant to construct a rational design and synthesis of dentritic Pt nanomaterials for glycerol electro-oxidation.

Generally, there are two synthetic routes to synthesize dentritic Pt nanomaterials: templateless and template routes.[16] The research on templateless synthesis reveals that Pt dentritic structures were favorable to the properties enhancement in electrocatalytic applications.[14,17−19] However, the templateless reaction process requires stricter conditions than template reaction.[16] Many reactions suffered from relatively high temperature, long duration, or complicated synthetic procedures to obtain uniform-morphology products.[16,20] As one of the most important techniques for the shape-controlled synthesis of Pt nanomaterials, templated synthesis is a powerful tool which can directly produce nanomaterials with desired nanoscale features that are otherwise difficult to obtain.[16] Still, the morphology of the nanomaterials synthesized by template strategies is generally similar to the template,[7,21] and few research reports were reported on the synthesis of the Pt nanoflower structure using one-dimensional (1D) materials as template.[22] Galvanic replacement is an effective method to generate hollow or novel nanostructures and tellurium nanowires (TeNWs) were widely used to form Pt nanostructures.[23−25] For example, in this specific reaction, it is relatively easy to synthesize Pt or alloys nanotubes (PtNTs)/porous NTs using TeNWs as a template.[6,26] However, it is difficult to transfrom TeNWs to nanobranch Pt nanomaterials completely, in general, due to the limitation of 1D nanostructures.[22] Furthermore, Pt nanobranches could be obtained with enriched edge and corner atoms, in high yield and in large quantities by inducing the aggravation of galvanic replacement.[3,27]

Herein, we demonstrated that the monomorphic single-crystalline Pt nanoflowers could be synthesized by galvanic replacement of TeNWs to form a Pt nanostructure completely as shown in Scheme 1. In this work, a comprehensive

Received: May 4, 2015
Accepted: July 30, 2015
Published: July 30, 2015

DOI: 10.1021/acsami.5b03826
ACS Appl. Mater. Interfaces 2015, 7, 17725−17730

Scheme 1. Schematic Illustration of the Evolution from TeNWs to Pt Nanoflowers with Well-Defined Morphologies

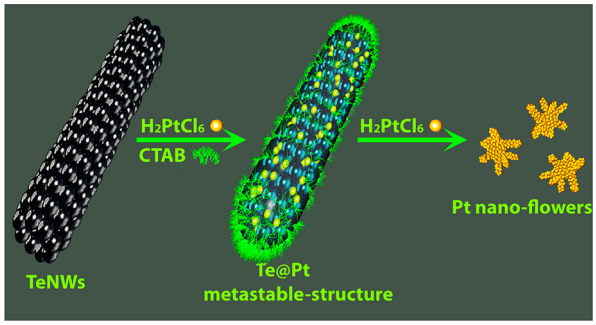

consideration of the synthesis factors were close integration of the possible mechanism, including the concentrations of CTAB and H_2PtCl_6 and the reaction temperature. The whole reaction process was in the water phase, and the as-prepared Pt products had well-defined morphologies. In the synthesis of Pt nanoflowers, 1 mL of as-prepared TeNWs was added into 6 mL of 27 mM CTAB, and then 0.3 mL of 1 mM H_2PtCl_6 (pH = 7) was injected into the mixture solution and mechanically stirred for 8 min. When the color of the solution turned amber, 0.7 mL of 1 mM H_2PtCl_6 (pH = 7) was injected again. The whole system was heated around 60 °C for about 30 min to obtain the Pt nanoflowers. Finally, after a centrifugation/wash cycle, the products were obtained, while only Pt nanowires were obtained without the addition of CTAB and the samples were characterized by TEM and UV−vis as shown in Figures S1 and S2.

EXPERIMENTAL SECTION

Preparation processes of TeNWs were performed as we reported previously.[7] As-prepared TeNWs (1 mL) were dispersed in CTAB solution (30 mM, 6 mL) for 10 min with constant magnetic stirring at 50 °C. Then a solution of H_2PtCl_6 (1 mM, 0.3 mL, pH = 7) was added into the mixture of TeNWs and CTAB, and the color of the mixture turned blue-black after 2 min. Another 0.7 mL of H_2PtCl_6 (1 mM, pH = 7) solution was quickly injected into the solution. The solution turned light amber after 30 min, and the mixture was subjected to a centrifugation/wash cycle to obtain Pt nanoflowers.

The dendrites sizes and morphologies of the as-synthesized Pt nanoflowers were examined by HRTEM (high-resolution transmission electron microscopy, JEM-2010FEF) and FE-SEM (field emission scanning electron microscopy, Zeiss, S-3500N). The energy-dispersive X-ray spectroscopy (EDS) analysis was also perfomed with a JEM-2010FEF at an accelerating voltage of 200 kV. The X-ray diffraction (XRD) analysis was performed on a Bruker D8 Advance X-ray diffractometer with Cu Kα radiation. The X-ray photoelectron spectra (XPS) analysis was tested by ESCALAB 250Xi and calibrated by the C 1s peak (284.6 eV).

The cyclic voltammograms (CV) were carried out in 0.5 M H_2SO_4 solution at a scan rate of 50 mV s^{-1}. The GOR was recorded in 0.5 M H_2SO_4 and 1 M $CH_2OHCHOHCH_2OH$ solution with the scan rate of 50 mV s^{-1}. Current density−time curves of the two catalysts were tested in 0.5 M H_2SO_4 + 1 M $CH_2OHCHOHCH_2OH$ solution at a constant potential of 0.6 V vs SCE. The detailed processes for all electrochemical experiments were presented in the Supporting Information. The catalyst loading of Pt nanoflowers and commercial Pt/C for all measurements were fixed to 21.9 μg_{Pt} cm^{-2} and 70.8 μg_{Pt} cm^{-2}.

RESULTS AND DISCUSSION

The X-ray diffraction (XRD) pattern of Pt nanoflowers in Figure S3 confirmed that the results were indexed to Pt with a face-centered cubic (fcc) structure (lattice constant a = 0.39 nm, JCPDS card no. 04-0802).[7] Energy dispersive X-ray (EDX) analyses in Figure S4 showed the TeNWs had been effectively transferred to Pt nanoflowers corresponding to the XRD pattern. These results indicated that the as-prepared nanostructure exclusively consisted of Pt. XPS spectra in Figure S5 present the Pt 4f core level for the Pt nanoflower. The core level of Pt 4f split into $4f_{5/2}$ and $4f_{7/2}$ states because of spin−orbital splitting.[28,29] The results of binding energy (BE) values at 74.166 and 70.8 eV correspond to Pt $4f_{5/2}$ and Pt $4f_{7/2}$.[29] However, compared with the Pt standard atlas, the peaks values of Pt $4f_{5/2}$ and Pt $4f_{7/2}$ were 0.034 and 0.1 eV less than those of Pt^0, respectively. The consequence might be caused by valency unsaturated atoms at edges and corners.[11,12,28,29] As seen in Figure 1, the TEM images of Pt nanoflowers under different

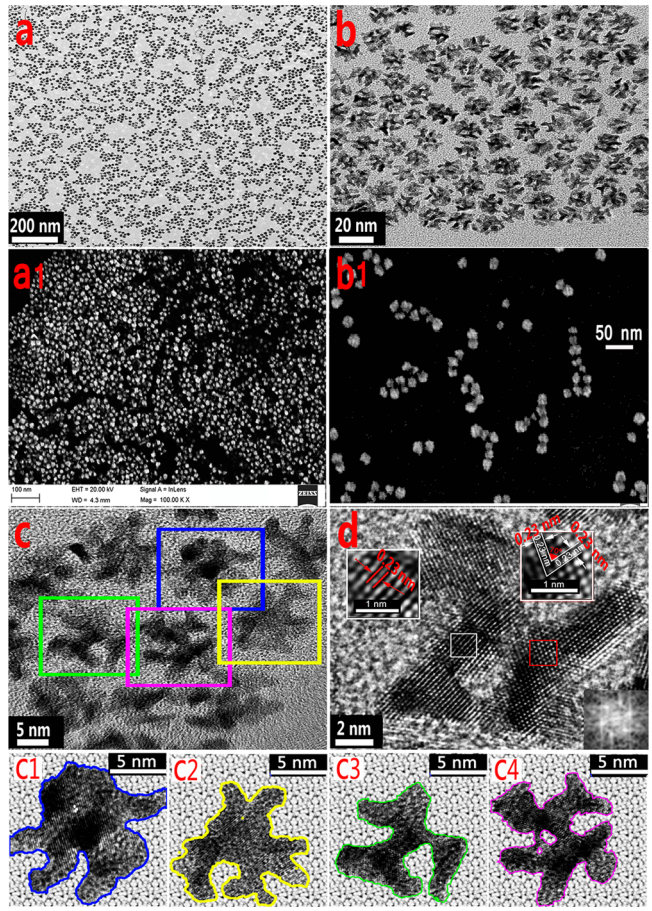

Figure 1. (a,b,c) Magnified TEM images of the Pt nanoflowers. (a1,b1) FESEM images of the Pt materials. (d) Fast Fourier transform (FFT) pattern and filtered images of the square area of an individual highly dentritic Pt nanoflower. (c1−4) Enlarged HRTEM images of Pt nanoflower with the clear outline.

magnifications showed an interesting structure with a remarkable distribution in size and shape. On the basis of the high resolution TEM (HRTEM) and FESEM depicted in Figure 1a−c, each nanoflower structure showed a bumpy surface of enriched valency unsaturated atoms at edges and corners, which could provide more catalytically active sites.[11,12] It could also be observed that the *d*-spacing of adjacent fringes for the nanoflower structure was 0.23 nm in Figure 1d, which was in agreement with a (111) plane spacing of fcc Pt.[19,30] Figure c1−4 showed the scale of each branch from a

DOI: 10.1021/acsami.5b03826
ACS Appl. Mater. Interfaces 2015, 7, 17725−17730

nanoflower was within 3 nm, which revealed that the highly crystalline Pt dentritic structure could deliver excellent performance electrocatalysts.[31]

As for the synthesis of Pt nanobranches, cetyltrimethylammonium bromide (CTAB) as the structure-directing agent could play a key role in the formation of a multidimension structure.[32,33] Owing to plus-to-minus charge interactions, CTA^+ might strongly combine with $PtCl_6^{2-}$, resulting in CTA^+-$PtCl_6^{2-}$, which could enrich $PtCl_6^{2-}$ around the Te nanomaterials and control the reaction kinetics.[7] The galvanic replacement reaction occurred as the equal electrical charge process as following eq 1:

$$PtCl_6^{2-} + Te + 3H_2O \rightarrow Pt + TeO_3^{2-} + 6Cl^- + 6H^+ \quad (1)$$

$$\frac{V_{m(Te)}}{V_{m(Pt)}} = \frac{M_{Te} \times \rho_{Pt}}{M_{Pt} \times \rho_{Te}} = 2.24 \quad (2)$$

According to eq 2, V_m is molar volume, M is molar mass, and ρ is density; the molar volume of Te (20.4 $cm^3\ mol^{-1}$) is 2.24 times larger than that of Pt (9.1 $cm^3\ mol^{-1}$).[6] There will be a 1.14 times of its own volume around each Pt atom, which is beneficial to generate a Te@Pt metastable structure as shown in Figure 2 (steps 1). The kinetics of alloying (steps 1) might

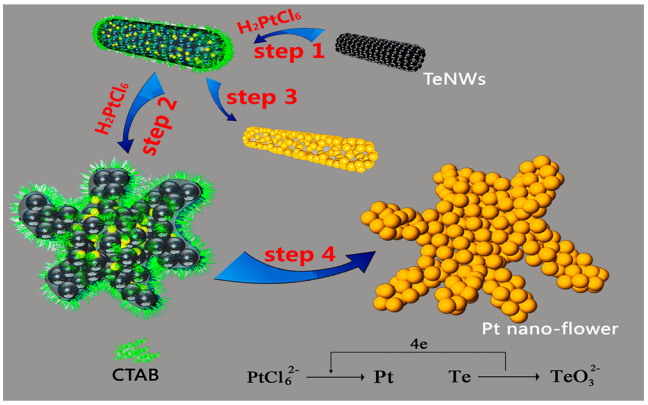

Figure 2. Simulation of mechanism of galvanic replacement from TeNWs to Pt nanoflowers with the equivalent charge reaction process.

be described by the derivation of Fick's second law of diffusion:[3,27]

$$k = \frac{1}{t} \cdot \ln \frac{1}{1 - \mathrm{erf}\frac{x}{\sqrt{2Dt}}} \quad (3)$$

Here, k is the rate constant, t is the reaction time, x is the distance of Pt from the Te@Pt metastable structure interface, and D is the dependence on the temperature as this reaction is conducted.[3] k would decrease with the passage of t at a certain temperature.

Figure 2 showed the main steps in the galvanic replacement reaction with H_2PtCl_6. When the 1 mM H_2PtCl_6 (pH = 7) was added into the mixture solution of as-prepared Te nanomaterials (Figure 3a) and CTAB, the galvanic replacement reaction would occur immediately between Te nanomaterials and Pt source[24] (Figure 2, steps 1). As a result, $PtCl_6^{2-}$ would be reduced to Pt atoms, generating an uneven discrete distribution of Pt&Te nanoshell on the surface of the Te nanomaterials.[7] Based on the stoichiometric relationship of the galvanic replacement reaction, eq 1, equivalent molar amounts

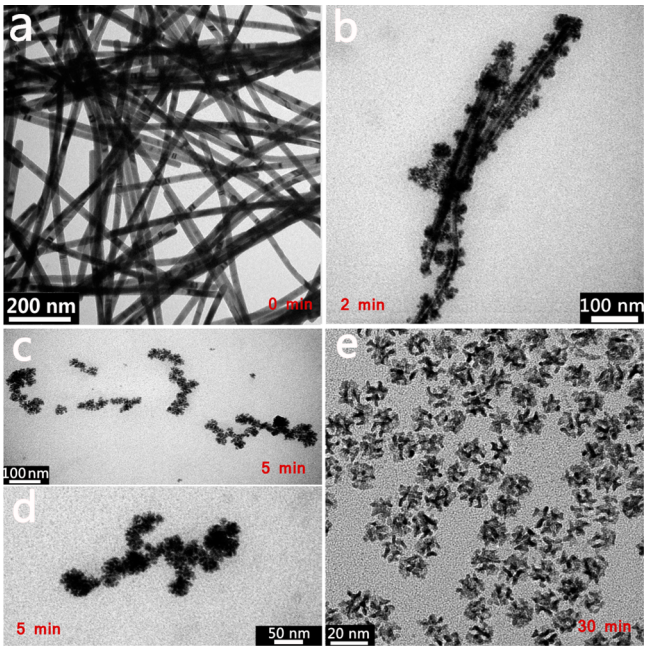

Figure 3. Schematic illustration of the progress from Te nanowires to Pt nanoflowers. TEM of (a) Te nanowires and (b) Pt&Te nanoshell on the surface of the Te nanowires which generates a hollow heterostructure. (c,d) Magnified TEM of Te@Pt heterostructure. (e) HRTEM of Pt nanoflowers.

of Pt atoms would be generated while Te nanomaterials dissolved into the solution. As the reaction continues, Te atoms in the Te@Pt heterostructure would be dissoloved and the Pt source around Te nanomaterials could quickly capture the electrons from the oxidation process of Te → TeO_3^{2-3}. The newly formed Pt atoms might be deposited in a special manner in the presence of CTAB, resulting in a hollow heterostructure[7,26] (Figure 3b), and the color of the solution turned blue gray. As the reaction continues, the driving force eq 3 for the reaction tends to drop due to the involvement of the composite structure and the decrease of reactants without addition of 1 mM H_2PtCl_6 (pH = 7).[34] Then unreacted tellurium atoms would be dissociation, owing to the Kirkendall effect and generated porous Pt nanotubes (Figure 2, steps 3). However, if another 700 μL of H_2PtCl_6 was injected into the solution, the aggravation of the galvanic replacement reaction would stimulate the decomposition of the hollow heterostructure, and the newly formed Pt atoms would adhere to the previous ones with Te atoms, which prefer an island growth mode[3,16,21] (Figure 2, step 2; Figure 3c,d). As a result, Pt nanoflowers were generated in the presence of CTAB (Figure 2, step 4; Figure 3e).

The ultraviolet absorption of a variety of reactants (CTAB, TeNWs, Te@Pt structure, Pt nanoflowers) was tested as the reaction progressed, and the data measured (Figure 4) with each stage corresponded to the product. In the ultraviolet absorption spectrum (Figure 4), an obvious decrease of peak intensity at 270 and 630 nm was observed, which indicated the replacement between TeNWs and the platinum precursor.[7] Furthermore, there was no absorption peak at 270 and 630 nm of the Pt nanoflowers curves, owing to the complete dissociation of TeNWs at the end of the reaction.

Pt-based nanodendrites with enriched edge and corner atoms are highly favorable for glycerol electrochemical oxidation in acid medium.[17] The electroactivity of the Pt nanoflower

DOI: 10.1021/acsami.5b03826
ACS Appl. Mater. Interfaces 2015, 7, 17725−17730

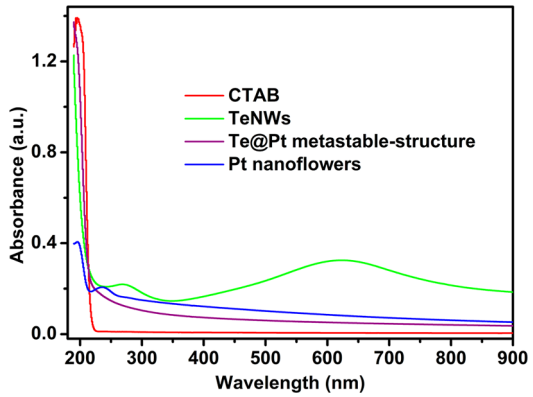

Figure 4. Absorption spectra of CTAB, TeNWs, Te@Pt metastable-structure, and Pt nanoflowers.

catalysts toward glycerol oxidation was tested by cyclic voltammetry (CV) and compared with that of commerial Pt/C (20% Pt). Specifically, Pt nanoflowers were washed by mixture of hot ethanol and acetone to remove the surfactant (CTAB). Figure S6 showed the CVs of the Pt nanoflowers and Pt/C catalysts in 0.5 M H_2SO_4 solution at room temperature. The electrochemical surface area (ECSA) of the catalyst was calculated based on the hydrogen adsorption charge in the potential region of −0.2 to 0.2 V vs SCE. The ECSA per g_{Pt} of Pt nanoflower (56.5 $m^2\ g^{-1}{}_{Pt}$) is lower than that of Pt/C (20% Pt, 77.1 $m^2\ g^{-1}{}_{Pt}$), mainly because of the large specific surface area of Pt nanoparticles (about 3−5 nm) in the Pt/C.[32] The amount of Pt was determined by inductively coupled plasma-atomic emission spectrometry (ICP-AES). To obtain the stability of ECSA per g_{Pt} of the two catalysts, six parallel tests were performed in 0.5 M H_2SO_4 solution at 50 mV s^{-1} under frequently changing potential. What's more, HRTEM of the after-cycles Pt nanoflowers shown in Figure S7 indicated the structural stability of the Pt nanomaterials. The consequence in Figure S8 showed that Pt nanoflowers have the better stability, which can be attributed to the steady structure.[35]

The electrocatalytic performance of the Pt nanoflowers for glycerol oxidation reaction (GOR) was tested and compared with Pt/C in 0.5 M H_2SO_4 + 1 M $CH_2OHCHOHCH_2OH$ solution at a scan rate of 50 mV s^{-1} as shown in Figure 5. It exhibited little difference in the shape of CV curves between the Pt nanoflower and Pt/C (20% Pt) catalysts CV curves of GOR, indicating the similar reaction pathway.[36] Besides, the changes in the absorption spectra of the substrate with catalytic time of 100 s, 200 s, 300 s, 400 s, 1000 s, 1500 s, 2000 s, 2500 s, 3000 s, 3500 s, and 4000 s were obtained by the ultraviolet−visible spectrophotometer, the absorbance of substrate (Figure 6)

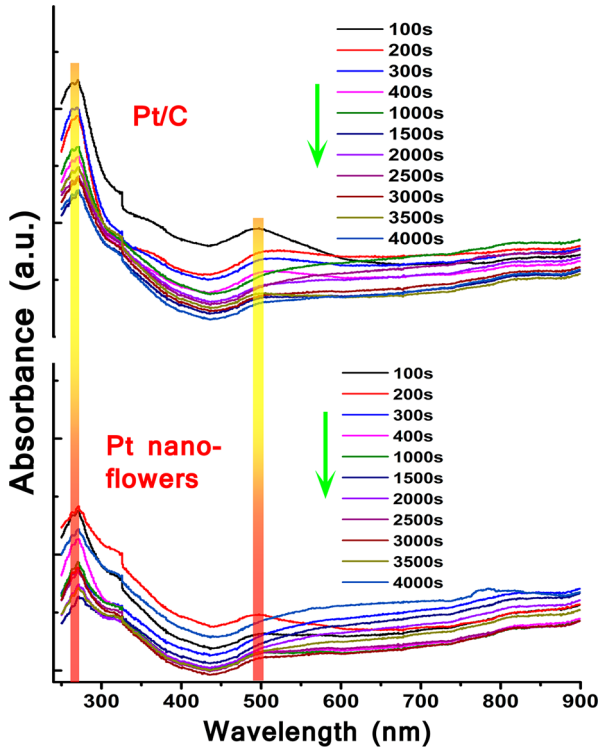

Figure 6. Changes in absorption spectra of substrate with catalytic time of 100 s, 200 s, 300 s, 400 s, 1000 s, 1500 s, 2000 s, 2500 s, 3000 s, 3500 s, and 4000 s (from top to bottom).

decreased with reaction time, and the main absorption peaks were the same, which confirmed the above conclusions. The significant results of two catalysts for glycerol oxidation at peak current were calculated and shown in Figure 5a. Clearly, the oxidation peak of Pt nanoflower (0.18 A mg^{-1}) is 2.6 times that of Pt/C (20% Pt, 0.07 A mg^{-1}), demonstrating that the

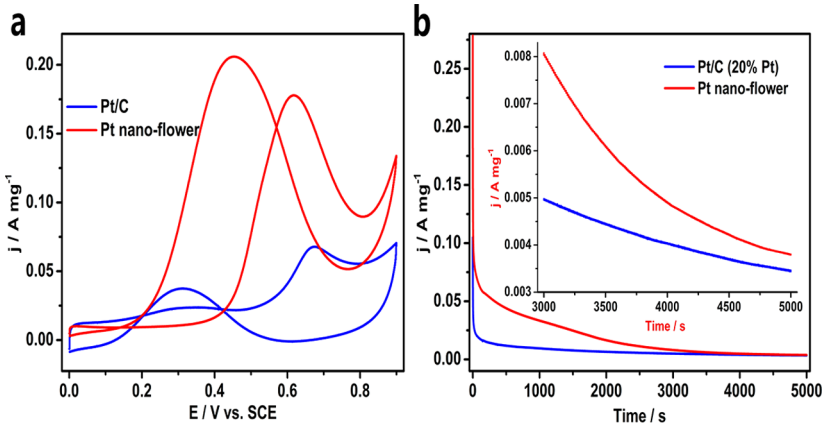

Figure 5. (a) Glycerol oxidation reaction catalyzed by the Pt nanoflowers and Pt/C catalysts in 0.5 M H_2SO_4 + 1 M $CH_2OHCHOHCH_2OH$ solution at 50 mV s^{-1}. (b) Current density−time curves of the two catalysts in 0.5 M H_2SO_4 + 1 M $CH_2OHCHOHCH_2OH$ solution at a constant potential 0.6 V vs SCE.

DOI: 10.1021/acsami.5b03826
ACS Appl. Mater. Interfaces 2015, 7, 17725−17730

dentritic structure could effectively enhance the inherent catalytic activity. Furthermore, chronoamperometry was chosen to assess the stability of the two catalysts in the presence of 1 M glycerol for 5000 s at a potential of 0.6 V vs SCE. Figure 5b displayed the higher current density of the Pt nanoflower than that of Pt/C. The rapid decay of current densities during the initial period was caused by the insufficiency of glycerol.

The potential-dependent motional resistance (ΔR_E) of glycerol electro-oxidation for Pt per mg might reveal that the structure of a Pt/C or Pt nanoflower changes frequently under changing potential.[37,38] CVs were tested in 0.5 M H_2SO_4 + 1 M $CH_2OHCHOHCH_2OH$ solution at 50 mV s^{-1} after the electrode coated catalysts were stable. Figure 7 showed different

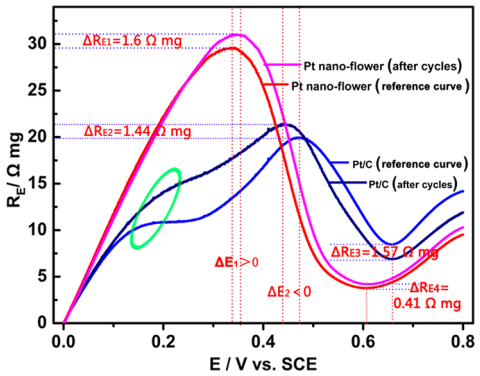

Figure 7. Potential-dependent motional resistance (R_E) of glycerol electro-oxidation for Pt per mg under changing potential frequently after the catalytic stability.

values of the peak resistance ΔR_E for the two catalysts. ΔR_{E2} = 1.44 Ω mg is smaller than ΔR_{E1} = 1.6 Ω mg while ΔE_1 is negative and ΔE_2 is positive, indicating that transmutation of the Pt/C structure might have occurred.[39] The Pt nanoparticle could detach from carbon and aggregate into a cluster and then increase the conductivity of the materials, which corresponded to the difference value of the peak resistance ΔR_{E2}. Furthermore, two peaks marked by a green elliptic-ring could further verify the above conclusions. The peak−valleys on the curves, ΔR_{E3} = 1.57 Ω mg and ΔR_{E4} = 0.41 Ω mg, reveal that Pt nanoflowers have better peformance than Pt/C during the glycerol electro-oxidation reaction. These results not only indicate the higher activity and stability of Pt nanoflower catalyst, but also demonstrate a high rate of valency unsaturated atoms could increase the activity of materials.

CONCLUSION

In conclusion, a highly crystallized Pt dentritic structure with a large amount of edge and corner atoms has been successfully synthesized through a template-broken synthesis strategy. A preliminary mechanism was proposed to explain the approach using 1D Te nanowires as a template. The process could be described as follows: aggravation of galvanic replacement could generate new structural materials when the molar volume of reactant is smaller than that of the template under reaction with equivalent charge. The as-prepared Pt nanoflower exhibited excellent performance toward glycerol electro-oxidation under acid conditions, demonstrating its potential application for direct glycerol fuel cells. Therefore, we believe this method is important for the template synthesis and could also provide a novel potential way to synthesize other noble metals/alloys for their advanced functional applications.

ASSOCIATED CONTENT

Supporting Information

The Supporting Information is available free of charge on the ACS Publications website at DOI: 10.1021/acsami.5b03826.

Experimental details (materials and reagents), XRD pattern of the Pt nanoflowers, EDS spectrum, CV curves in 0.5 M H_2SO_4 solution, ECSA per g_{Pt} for Pt nanoflowers, and Pt/C (20% Pt) (PDF)

AUTHOR INFORMATION

Corresponding Author

*E-mail: hyhan@mail.hzau.edu.cn.

Notes

The authors declare no competing financial interest.

ACKNOWLEDGMENTS

We acknowledge financial support from the National Natural Science Foundation of China (21375043, 21175051).

REFERENCES

(1) Peng, Z.; Yang, H. Designer platinum nanoparticles: Control of Shape, Composition in Alloy, Nanostructure and Electrocatalytic Property. *Nano Today* **2009**, *4*, 143−164.

(2) Dasgupta, N. P.; Sun, J.; Liu, C.; Brittman, S.; Andrews, S. C.; Lim, J.; Gao, H.; Yan, R.; Yang, P. 25th Anniversary Article: Semiconductor Nanowires-Synthesis, Characterization, and Applications. *Adv. Mater.* **2014**, *26*, 2137−2184.

(3) Xia, X.; Wang, Y.; Ruditskiy, A.; Xia, Y. 25th Anniversary Article: Galvanic Replacement: A Simpleand Versatile Route to Hollow Nanostructures with Tunable and Well-Controlled Properties. *Adv. Mater.* **2013**, *25*, 6313−6333.

(4) Guo, S.; Wang, E. Noble Metal Nanomaterials: Controllable Synthesis and Application in Fuel Cells and Analytical Sensors. *Nano Today* **2011**, *6*, 240−264.

(5) Cao, L.; Scheiba, F.; Roth, C.; Schweiger, F.; Cremers, C.; Stimming, U.; Fuess, H.; Chen, L.; Zhu, W.; Qiu, X. Novel Nanocomposite Pt/RuO_2 Nanotube Catalysts for Direct Methanol Fuel Cells. *Angew. Chem., Int. Ed.* **2006**, *45*, 5315−5319.

(6) Liang, H.; Liu, S.; Gong, J.; Wang, S.; Wang, L.; Yu, S. Ultrathin Te Nanowires: An Excellent Platform for Controlled Synthesis of Ultrathin Platinum and Palladium Nanowires/Nanotubes with Very High Aspect Ratio. *Adv. Mater.* **2009**, *21*, 1850−1854.

(7) Zuo, Y.; Cai, K.; Wu, L.; Li, T.; Lv, Z.; Han, H. Spiny-Porous Platinum Nanotubes with Enhanced Electrocatalytic Activity for Methanol Oxidation. *J. Mater. Chem. A* **2015**, *3*, 1388−1391.

(8) Leong, G. J.; Schulze, M. C.; Strand, M. B.; Maloney, D.; Richards, R. M. Shape-Directed Platinum Nanoparticle Synthesis: Nanoscale Design of Novel Catalysts. *Appl. Organomet. Chem.* **2014**, *28*, 1−17.

(9) Xia, Y. Shape-Controlled Synthesis of Metal Nanocrystals: Simple Chemistry Meets Complex Physics? *Angew. Chem., Int. Ed.* **2009**, *48*, 60−103.

(10) Zhang, L.; Li, N.; Gao, F.; Hou, L.; Xu, Z. Insulin Amyloid Fibrils: An Excellent Platform for Controlled Synthesis of Ultrathin Superlong Platinum Nanowires with High Electrocatalytic Activity. *J. Am. Chem. Soc.* **2012**, *134*, 11326−11329.

(11) Wang, L.; Yamauchi, Y. Block Copolymer Mediated Synthesis of Dentritic Platinum Nanoparticles. *J. Am. Chem. Soc.* **2009**, *131*, 9152−9153.

(12) Wang, L.; Yamauchi, Y. Rapid and Efficient Synthesis of Platinum Nanodendrites with High Surface Area by Chemical Reduction with Formic Acid. *Chem. Mater.* **2010**, *22*, 2835−2841.

(13) Hu, J.; Tanabe, M.; Sato, J.; Uosaki, K.; Ikeda, K. Effects of Atomic Geometry and Electronic Structure of Platinum Surfaces on Molecular Adsorbates Studied by Gap-Mode SERS. *J. Am. Chem. Soc.* **2014**, *136*, 10299−10307.

DOI: 10.1021/acsami.5b03826
ACS Appl. Mater. Interfaces 2015, 7, 17725−17730

(14) Martinez-Rodriguez, R. A.; Vidal-Iglesias, F. J.; Solla-Gullon, J.; Cabrera, C. R.; Feliu, J.-M. Synthesis of Pt Nanoparticles in Water-in-Oil Microemulsion: Effect of HCl on Their Surface Structure. *J. Am. Chem. Soc.* **2014**, *136*, 1280−1283.
(15) Yu, E. H.; Krewer, U.; Scott, K. Principles and Materials Aspects of Direct Alkaline Alcohol Fuel Cells. *Energies* **2010**, *3*, 1499−1528.
(16) Liu, Y.; Goebl, J.; Yin, Y. Templated Synthesis of Nanostructured Materials. *Chem. Soc. Rev.* **2013**, *42*, 2610.
(17) Shen, Y.; Xi, J. Electrocatalytic Activity of Pt Subnano/Nanoclusters Stabilized by Pristine Graphene Nanosheets. *Phys. Chem. Chem. Phys.* **2014**, *16*, 21609.
(18) Gong, M.; Fu, G.; Lu, T. Autocatalysis and Selective Oxidative Etching Induced Synthesis of Platinum-Copper Bimetallic Alloy Nanodendrites Electrocatalysts. *ACS Appl. Mater. Interfaces* **2014**, *6*, 7301−7308.
(19) You, H.; Fang, J. Free-Standing Pt-Au Hollow Nanourchins with Enhanced Activity and Stability for Catalytic Methanol Oxidation. *ACS Catal.* **2014**, *4*, 2829−2835.
(20) Chen, C.; Kang, Y.; Li, Y.; Markovic, N. M.; Somorjai, G.-A.; Yang, P.; Stamenkovic, V. R. Highly Crystalline Multimetallic Nanoframes with Three-Dimensional Electrocatalytic Surfaces. *Science* **2014**, *343*, 1339−1343.
(21) Yang, S.; Luo, X. Mesoporous Nano/Micro Noble Metal Particles: Synthesis and Applications. *Nanoscale* **2014**, *6*, 4438−4457.
(22) Lin, Z.; Chang, H. Facile Synthesis of Catalytically Active Platinum Nanosponges, Nanonetworks, and Nanodendrites. *Chem. - Eur. J.* **2009**, *15*, 4656−4662.
(23) Liu, J.; Huang, W.; Gong, M.; Yu, S. H. Ultrathin Hetero-Nanowire-Based Flexible Electronics with Tunable Conductivity. *Adv. Mater.* **2013**, *25*, 5910−5915.
(24) Xu, L.; Liang, H.; Li, H.; Yu, S. H. Understanding the Stability and Reactivity of Ultrathin Tellurium Nanowires in Solution: An Emerging Platform for Chemical Transformation and Material Design. *Nano Res.* **2015**, *8*, 1081−1097.
(25) Wang, K.; Yang, Y.; Liang, H.; Yu, S. H. First Sub-Kilogram-Scale Synthesis of High Quality Ultrathin Tellurium Nanowires. *Mater. Horiz.* **2014**, *1*, 338.
(26) Cai, K.; Lv, Z.; Han, H. Aqueous Synthesis of Porous Platinum Nanotubes at Room Temperature and Their Intrinsic Peroxidase-Like Activity. *Chem. Commun.* **2013**, *49*, 6024.
(27) Sun, Y.; Xia, Y. Mechanistic Study on the Replacement Reaction between Silver Nanostructures and Chloroauric Acid in Aqueous Medium. *J. Am. Chem. Soc.* **2004**, *126*, 3892−3901.
(28) Xu, C.; Li, Q.; Liu, Y.; Wang, J.; Geng, H. Hierarchical Nanoporous PtFe Alloy with Multimodal Size Distributions and Its Catalytic Performance toward Methanol Electrooxidation. *Langmuir* **2012**, *28*, 1886−1892.
(29) Li, H.; Zhao, S.; Gong, M.; Cui, C.; Yu, S. Ultrathin PtPdTe Nanowires as Superior Catalysts for Methanol Electrooxidation. *Angew. Chem., Int. Ed.* **2013**, *52*, 7472−7476.
(30) Kim, Y.; Hong, J.; Lee, Y.; Kim, M.; Han, S. Synthesis of AuPt Heteronanostructures with Enhanced Electrocatalytic Activity toward Oxygen Reduction. *Angew. Chem., Int. Ed.* **2010**, *49*, 10197−10201.
(31) Zhao, D.; Xu, B. Enhancement of Pt Utilization in Electrocatalysts by Using Gold Nanoparticles. *Angew. Chem., Int. Ed.* **2006**, *45*, 4955−4959.
(32) Xia, B.; Lou (David), X. W. Self-Supported Interconnected Pt Nanoassemblies as Highly Stable Electrocatalysts for Low-Temperature Fuel Cells. *Angew. Chem., Int. Ed.* **2012**, *51*, 7213−7216.
(33) Lim, B.; Xia, Y. Metal Nanocrystals with Highly Branched Morphologies. *Angew. Chem., Int. Ed.* **2011**, *50*, 76−85.
(34) Skrabalak, S. E.; Sun, Y.; Xia, Y. Gold Nanocages: Synthesis, Properties, and Applications. *Acc. Chem. Res.* **2008**, *41*, 1587−1595.
(35) Li, Y.; Zhu, E.; McLouth, T.; Huang, Y. Stabilization of High-Performance Oxygen Reduction Reaction Pt Electrocatalyst Supported on Reduced Graphene Oxide/Carbon Black Composite. *J. Am. Chem. Soc.* **2012**, *134*, 12326−12329.
(36) Zalineeva, A.; Padilla, M.; Martinez, U.; Atanassov, P. B. Self-Supported PdxBi Catalysts for the Electrooxidation of Glycerol in Alkaline Media. *J. Am. Chem. Soc.* **2014**, *136*, 3937−3945.
(37) John, J.; Hugar, K. M.; Abruna, H. D. An Electrochemical Quartz Crystal Microbalance Study of a Prospective Alkaline Anion Exchange Membrane Material for Fuel Cells: Anion Exchange Dynamics and Membrane Swelling. *J. Am. Chem. Soc.* **2014**, *136*, 5309−5322.
(38) Worz, N.; Brandner, A.; Claus, P. Platinum-Bismuth-Catalyzed Oxidation of Glycerol: Kinetics and the Origin of Selective Deactivation. *J. Phys. Chem. C* **2010**, *114*, 1164−1172.
(39) Shao-Horn, Y.; Sheng, W. C.; Chen, S.; Ferreira, P. J.; Holby, E. F.; Morgan, D. Instability of Supported Platinum Nanoparticles in Low-Temperature Fuel Cells. *Top. Catal.* **2007**, *46*, 285.

DOI: 10.1021/acsami.5b03826
ACS Appl. Mater. Interfaces 2015, 7, 17725−17730